LiDAR-Camera Integration for High Precision Airborne Mapping

Bernhard Schachinger[1], Mohamed Mostafa[2], Nico Jaeger[2], Armin Borovcnik[1], Jonathan Hall Riaza[1] and Marc Muick[1]

[1] Vexcel Imaging GmbH, Anzengrubergasse 8, 8010 Graz, Austria – {bernhard.schachinger, armin.borovcnik, jonathan.riaza, marc.muick}@vexcel-imaging.com

[2] Trimble Applanix, 85 Leek Cr., Richmond Hill, Ontario, Canada L4B 3B3 {mohamed_mostafa, nico_jaeger}@trimble.com

KEYWORDS: photogrammetry, LiDAR, digital twin, hybrid system, trajectory

ABSTRACT

Airborne mapping projects are vital for modern infrastructure and urban planning. The primary goal is to produce and update base maps that serve as essential tools in both public and private sectors to enable a variety of applications. As a result, large airborne surveying and mapping projects are conducted regularly around the world to acquire high-resolution aerial imagery and LiDAR point clouds that can encompass entire countries, states, provinces, counties, or cities. By leveraging advanced technology and navigating the complexities of LiDAR, photogrammetric, and geodetic systems, these projects can significantly contribute to the development and maintenance of accurate base maps, ultimately enhancing decision-making processes across sectors.

This paper presents tests of a new fully integrated multi-sensor airborne system that comprises LiDAR, multiple cameras, inertial measuring unit (IMU), GNSS, and their associated software for data acquisition, processing, integration, calibration, and map production. The technical analysis presented in this paper focuses on multi-sensor system integration that statistically addresses a multi-stream of LiDAR ranges, pixels from multiple cameras, position and orientation of each LiDAR range and each photo center derived from the GNSS/IMU trajectory. The study evaluates two trajectory processing approaches: Post-Processed Kinematic (PPK) using a single base station and Trimble Post-Processed RTX (PP-RTX). Real-world datasets collected with the Vexcel Imaging UltraCam Dragon in Austria and the United States were used to assess system performance under operational conditions. Results demonstrate that both Single Base and PP-RTX approaches provide reliable trajectory processing and consistent georeferencing accuracy for both imagery and LiDAR data.

1. INTRODUCTION

Reliable georeferencing is essential for accurately integrating airborne image and LiDAR data. Over the past three decades, an increasing number of simultaneous multi-sensor systems have been developed and deployed, typically featuring multi-camera arrays or LiDAR sensors integrated with embedded georeferencing systems. This integration relies fundamentally on robust GNSS/IMU setups. By employing aided-inertial Kalman filter architectures and post-processing techniques (Scherzinger et al, 2018; Hutton et al, 2004), these systems provide the precise exterior orientation necessary for both sensor types. Numerous studies have confirmed the accuracy of this approach across a variety of airborne photogrammetric applications (e.g., Mostafa, 2001; Mostafa and Schwarz, 2001; Mostafa and Hutton, 2004; Casella et al, 2006; Ip et al., 2006, 2007; Colomina & Blazquez, 2014; Dohr et al, 2022; Gruber and Wiechert, 2017; Gruber et al, 2022).

In operational practice, GNSS/IMU trajectories are typically processed using a Post-Processed Kinematic (PPK) approach based on observations from a nearby reference station. This single-base workflow has become the standard solution due to its ability to deliver high positioning accuracy under favourable conditions (c.f., Schwarz, et al, 1993; Mostafa and Schwarz, 1997).

However, this approach depends on the availability of suitable ground infrastructure. In many mapping projects, particularly in remote or sparsely instrumented regions, no reference station data are accessible within an appropriate distance. Setting up a temporary base station for such projects requires additional effort in terms of logistics, cost, and quality control. These limitations have motivated the adoption of alternative positioning strategies that are less dependent on local reference data.

One such alternative is the use of globally derived correction services within a Precise Point Positioning (PPP) framework. The PP-RTX method, implemented in Trimble Applanix processing software, employs precise satellite orbit and clock corrections generated from a worldwide network of tracking stations. These corrections are applied directly during trajectory computation, enabling GNSS/IMU processing without the need for a local base station. This concept offers increased flexibility in data acquisition and has the potential to streamline airborne survey operations.

The present study investigates the influence of these two processing strategies on airborne mapping data collected with the UltraCam Dragon system. Trajectories obtained from conventional PPK single-base processing are compared with those derived from PP-RTX processing, and their effects on the resulting geospatial products are analysed. In addition, the positional agreement between image-based measurements and lidar data is evaluated to assess the consistency between both sensor types. The aim of this work is to quantify the differences between the two trajectory solutions and to determine whether the PPP-based approach provides results comparable to the established PPK workflow. At the same time, the study examines the geometric compatibility of aerial imagery and lidar data when processed under these different conditions.

2. TECHNOLOGY DESCRIPTION

This work describes results from an investigation based on data captured with the UltraCam Dragon from Vexcel Imaging (Figure 1), a hybrid sensor renowned in the industry for

https://doi.org/10.5194/isprs-archives-XLIX-B1-2026-323-2026 |

consistent quality. While the current version of the system is 4.2, the data for this investigation was captured with a Dragon 4.1.
The concept of the system is the same for both, whereas only parameters for the camera components have changed. Therefore, it is expected that the results which are based on data from 4.1 also apply to data from 4.2.

Figure 1: UltraCam Dragon 4.2

2.1 UltraCam Dragon 4.2

The UltraCam Dragon 4.2 is an integrated hybrid multi-camera/LiDAR system designed for simultaneous LiDAR and imagery data acquisition. The system includes Nadir RGB and NIR cameras, 4 RGB oblique cameras and a professional grade LiDAR system, bridging the gap between passive and active remote sensing technologies.

At its core, the payload features a comprehensive optical suite-including Nadir RGB and near-infrared (NIR) sensors for high-resolution, top-down mapping, alongside four RGB oblique cameras designed to capture intricate structural facades and street-level perspectives. Complementing this optical array is a powerful and unique LiDAR system from RIEGL. Table 1 lists an overview of system specifications.

Table 1: System Specifications

System Component	Description
Imaging sensor	Sony IMX811 CMOS 247 Megapixels
Nadir Cameras	1 RGB + 1 NIR
Oblique Cameras	4 RGB cameras
Image size Nadir	19,136 x 12,736 pixels
Image size Oblique	19,136 x 12,736 pixels
Image capture rate	Up to 1 frame per 0.7 seconds
Lens (Nadir Camera)	• 51 mm lens • 38.8° along-track FOV • 55.8° across-track FOV
Lens (Oblique)	• 82 mm lens • 12° along-track FOV • 12° - 24° across-track FOV
Pixel size	2.81 µm
LiDAR	• Riegl VQ-680 • Pulse Repetition Rate 2.4 MHz • 50-500 lines per second
LiDAR Scan Geometry	Multi-axis with 5 viewing angles (−20°, −10°, 0°/true nadir, +10°, +20°)
LiDAR FOV	• 40° along-track FOV • 60° across-track FOV
Georeferencing	Trimble AP+ 60

As detailed in Table 1, a defining characteristic of the Dragon 4.2's architecture is the integration of the multi-axis LiDAR scanner. Unlike traditional LiDAR systems that rely predominantly on a single nadir-oriented pulse, this system utilizes a complex scan geometry with five distinct viewing angles along the flight trajectory (−20°, −10°,0 0°, +10°, and +20°). This multi-directional laser scanning works in perfect synergy with the system's four oblique cameras as shown in Figure 2. While the oblique sensors capture the high-resolution visual textures of building facades and vertical structures, the multi-angle LiDAR simultaneously maps the underlying physical geometry.

By eliminating targets from multiple perspectives, the system minimizes "LiDAR shadows"—areas that would typically be occluded by tall buildings in narrow urban canyons or by dense tree canopies.

This synchronized, multi-angle approach ensures the generation of a highly uniform, dense point cloud, which is critical for extracting precise digital surface models (DSMs) and constructing seamless 3D digital twins.

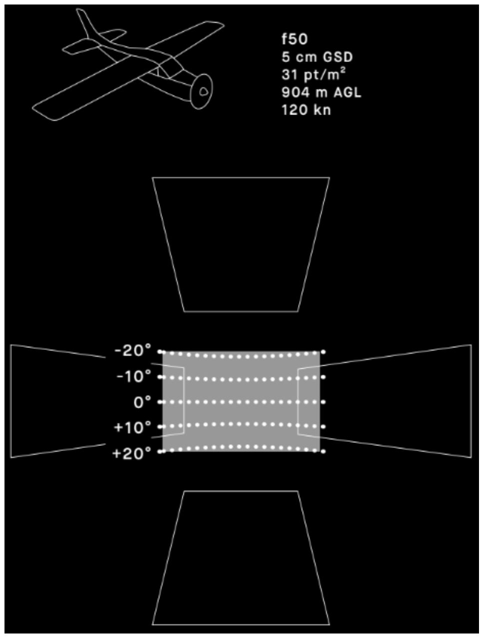

Figure 2: UltraCam Dragon Nadir & Oblique Imaging Footprint and LiDAR Scan Lines

2.2 Data Processing Pipeline

The simultaneous acquisition of multi-spectral imagery and high-density LiDAR necessitates a robust and highly automated processing pipeline as shown in Figure 3.

The data processing methodology for the UltraCam Dragon 4.2 workflow generally follows a multi-stage sensor fusion approach, ensuring that the image data perfectly aligns with the point cloud data.

The standard pipeline involves the following key phases:

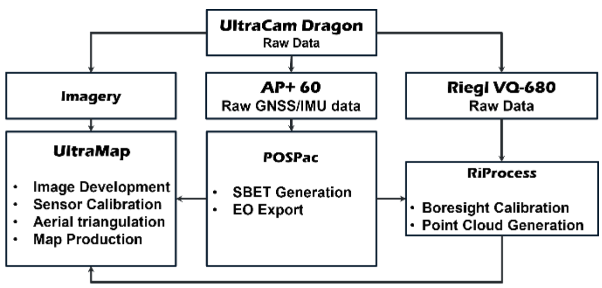

Figure 3: UltraCam Dragon Data Processing Workflow

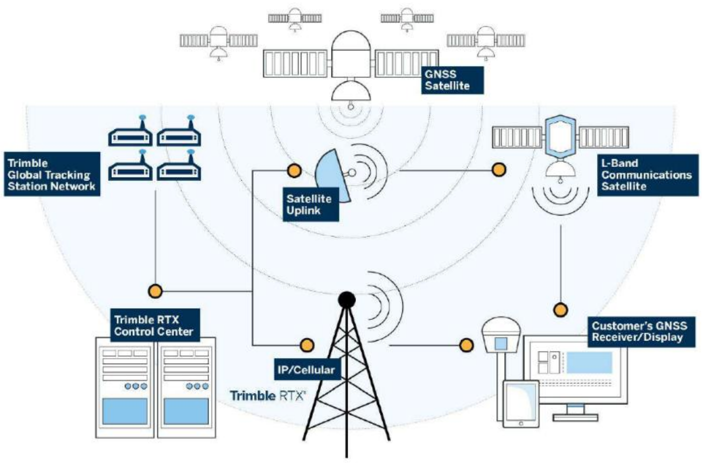

Figure 4: Trimble RTX - How Does It Work?

2.2.1 Trajectory Processing

Initial processing begins with the integration of Global Navigation Satellite System (GNSS) and Inertial Measurement Unit (IMU) data to calculate a highly precise post-processed kinematic (PPK) flight trajectory. This establishes the absolute spatial positioning and orientation for every captured image and LiDAR range.

2.2.2 Image processing

Raw image data is processed using Vexcel's proprietary algorithms in the software UltraMap, notably True Pixel Processing (TPP) with Adaptive Motion Compensation (AMC). TPP minimizes noise and optimizes sharpness, while AMC mitigates image blur caused by aircraft movement (Dohr et al., 2022). The workflow in UltraMap ensures homogeneous radiometric adjustment of the image block with the help of automated color balancing.

2.2.3 LiDAR Calibration and Point Cloud Processing

The raw LiDAR data is decoded and georeferenced using the precise trajectory. A rigorous LiDAR data adjustment is then accomplished using LiDAR QC software which aligns the point cloud globally from overlapping flight lines, correcting any minor systematic discrepancies between the multi-axis sweeps. The result is a dense, geometrically verified, and adjusted 3D point cloud.

2.2.4 Sensor Fusion and Co-registration

Because both active and passive sensors operate on the same rigid mount and share a unified temporal reference, co-registration is exceptionally accurate. The calibrated RGB and NIR imagery can be mapped onto the LiDAR point cloud for colorization and other tasks.

2.2.5 Deliverable Extraction

The finalized imagery and point cloud serve as foundational datasets. From this, advanced algorithms generate derivative products, including highly accurate Digital Surface Models (DSMs), Digital Terrain Models (DTMs), and seamless, fully textured 3D meshes (digital twins).

3. ACCURACY ASSESSMENT FLIGHTS

To assess the system accuracy, two test flights were flown:

1. Greeley, Colorado/USA
2. Gleisdorf, Austria

To evaluate the performance of the UltraCam Dragon, dedicated flight missions were conducted focusing on system calibration and subsequent accuracy assessment.

While each of these flights serves a distinct analytical purpose and will be examined individually in the following subsections, they share a unified data processing workflow.

Therefore, to provide a foundational understanding of the methodology, the system calibration protocols and baseline processing procedures will be detailed first.

To ensure the absolute positional accuracy required for the simultaneous acquisition of LiDAR and imagery, the Dragon relies on the high-performance Trimble AP+ 60 GNSS/IMU direct georeferencing system.

This unit offers two primary operational workflows for computing airborne trajectory data, providing flexibility based on specific project requirements and geographic constraints.

The traditional Post-Processed Kinematic (PPK) approach pairs the aircraft's onboard GNSS data with a local base station deployed within the project area, or a nearby Continuously Operating Reference Station (CORS).

By calculating differential corrections over relatively short baselines (within 30 Km), this method yields ultra-tight, centimeter-level accuracy. It is the preferred approach for highly localized mapping projects.

Trimble Post-Processed RTX (PP-RTX), shown in Figure 4, is an alternative to local base stations, leveraging a global network of reference stations to provide precise satellite orbit and clock corrections directly to the trajectory processing POSPac software.

https://doi.org/10.5194/isprs-archives-XLIX-B1-2026-323-2026 | © Author(s) 2026. CC BY 4.0 License.

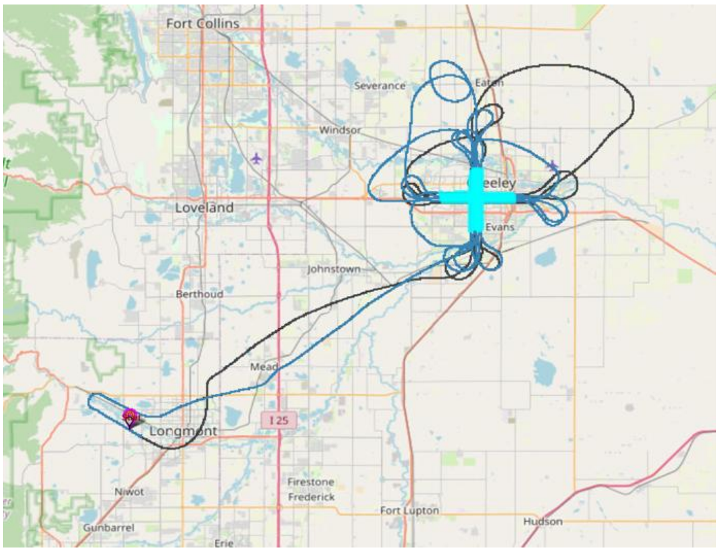

Figure 5: Flight Trajectory - Greeley, CO, USA

This eliminates the logistical overhead and baseline limitations associated with physical base stations. PP-RTX is particularly advantageous for large-scale, wide-area mapping or remote projects where deploying a dedicated base station is logistically impractical, maintaining the high absolute accuracies necessary for rigorous 3D modeling without localized infrastructure. Table 2 lists the accuracy specifications for both Single Base and RTX methods.

Table 2: Trimble AP+ 60 Absolute Accuracy Specifications

	PPK-Single Base	PP-RTX
Position (m)	0.02 H 0.05 V	0.03 H 0.06 V
Velocity (m/s)	0.005	0.005
Roll & Pitch (deg)	0.0025	0.0025
True Heading (deg)	0.005	0.005

Figure 6 illustrates the data processing workflow used for accuracy assessment purposes.

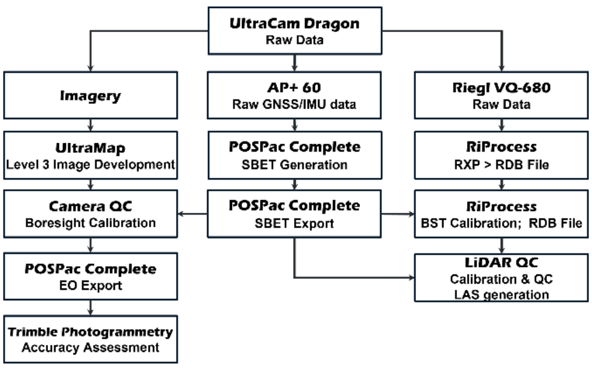

Figure 6: Data Processing Workflow used for Accuracy Assessment

3.1 Test Flight #1 (Greeley, Colorado, USA)

To facilitate system calibration and subsequent accuracy assessments, flight missions utilizing the UltraCam Dragon 4.1 were conducted over Greeley, Colorado/USA. The flight trajectory, illustrated in Figure 5, consisted of two distinct altitudes: approximately 1,000 meters and 2,000 meters Above Ground Level (AGL).

These specific flying heights were selected to yield a Ground Sample Distance (GSD) of 5 cm for the lower altitude and 10 cm for the higher altitude. Within Figure 5, the light blue triangles indicate the precise airborne exposure locations. At each of these designated coordinates, the system synchronously captured both the nadir and oblique imagery. The aircraft was flown at 145 knots (75 m/s).

In parallel with the synchronous image capture, the integrated LiDAR continuously collected topographical data across both flight profiles. As anticipated, the distinct flying heights of 1,000 m and 2,000 m AGL directly influenced the resulting LiDAR point density and swath width.

For instance, the 1,000 m altitude yielded a highly dense point cloud of almost 30 points per square meter - a density ideal for fine structural extraction that perfectly complements the 5 cm GSD imagery.

To evaluate the absolute geometric accuracy of the data, a total of 19 combined control and check points, coordinatized in the ITRF 2008 reference frame (epoch Jan 1st, 2018), were established within the flight area. They were also used to assess the LiDAR point cloud data shown in Figure 7.

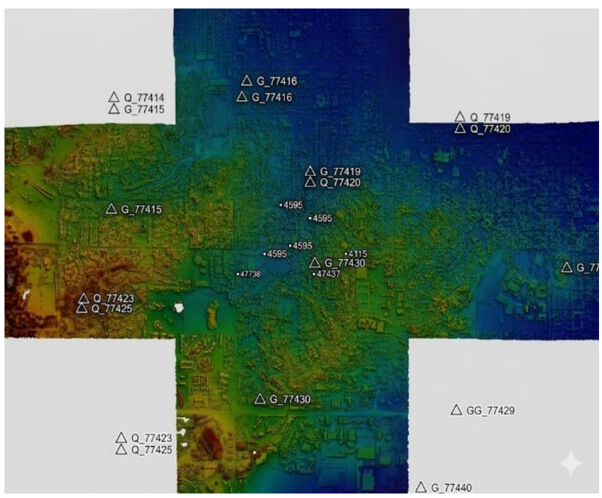

Figure 7: LiDAR Point Cloud - Greeley, CO, USA

During the trajectory processing phase, two distinct georeferencing methodologies were employed to establish a comparative baseline.

First, a nearby Continuously Operating Reference Station (CORS), located within 30 km of the flight area center, was utilized in a single base station scenario (PPK) to compute the primary flight trajectory.

Subsequently, a second trajectory for the exact same flight was computed entirely independently using Trimble's PP-RTX service.

By directly comparing these two distinct trajectories, this study aims to rigorously assess the absolute positional accuracy and operational viability of the Trimble RTX solution compared to traditional localized single base station processing.

3.1.1 Single Base & PP-RTX Processing Results

POSPac software was utilized to process the baseline trajectory for Flight #1 (the Greeley, CO dataset) using the traditional single-base approach, leveraging the CORS station located within 30 km of the project center.

The POSPac-estimated positioning accuracy and orientation accuracy are illustrated in Figure 8 and Figure 9, respectively. To rigorously evaluate the quality of this solution, the forward-reverse separation was analyzed (Figure 10).

POSPac's tightly coupled GNSS/INS integration algorithm processes the kinematic data sequentially in a forward direction through the time domain, and then backward in reverse. Comparing these two solutions provides an independent metric for assessing the internal consistency and overall accuracy of the Smoothed Best Estimate of Trajectory (SBET).

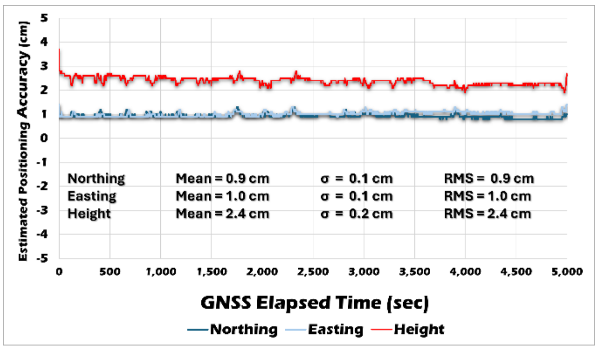

Figure 8: Estimated Positioning Accuracy Using a Single Base Station (using a CORS Station within 30 km) Greeley, CO, USA Dataset

Following the traditional base station processing, the identical raw flight data from Flight #1 (the Greeley, CO dataset) was re-processed in POSPac utilizing the Trimble Post-Processed RTX (PP-RTX) service.

This approach eliminates the dependency on the local 30 km CORS single base station. The resulting POSPac-estimated positioning accuracy for this independent, RTX-derived trajectory is illustrated in Figure 11.

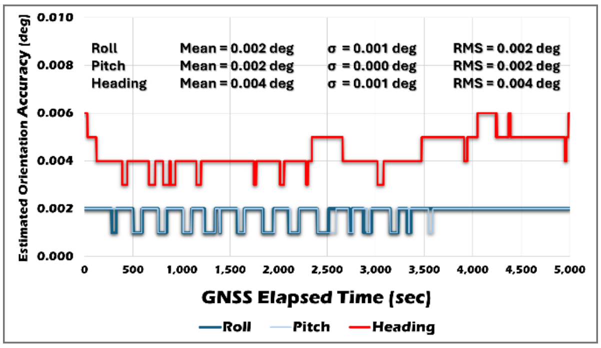

Figure 9: Estimated Orientation Accuracy Using a Single Base Station (using a CORS Station within 30 km) Greeley, CO, USA Dataset

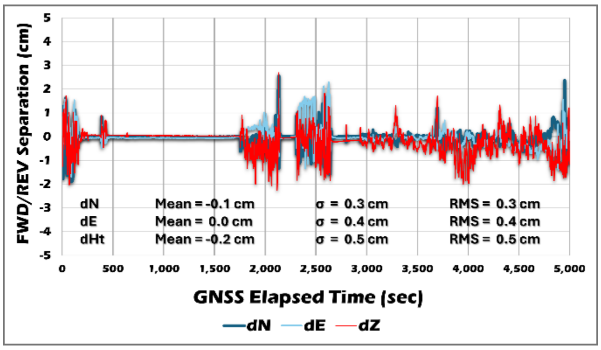

Figure 10: Trajectory Forward - Reverse Separation Greeley, CO, USA Dataset

Having processed the identical flight data through two distinct georeferencing methodologies—the localized single-base station approach and the global PP-RTX solution—a direct spatial comparison was conducted.

The absolute positional differences between these two independently derived trajectories were computed along the flight path, with the resulting coordinate deltas illustrated in Figure 11.

Based on the trajectory analysis presented in this section, the following key observations can be derived from Figure 8 through Figure 12:

- **Single Base Station Performance:** The estimated RMS positioning accuracy utilizing a single base station is approximately 20% of the Ground Sample Distance (GSD) in both the Northing and Easting components, and approximately 50% of the GSD in height. Additionally, the forward-Reverse Separation RMS is well within 10% of the GSD.
- **PP-RTX Performance:** Similarly, the estimated RMS positioning accuracy utilizing the independent PP-RTX method is approximately 30% of the GSD in both Northing and Easting, and roughly 75% of the GSD in height.
- **Hardware Compliance:** The estimated positioning accuracies for both the single base station and PP-RTX methodologies fall well within the stringent accuracy specifications of the Trimble AP+ 60, as detailed previously in Table 2.

- **Trajectory Variance**: The absolute coordinate difference between the two computed trajectories is minimal - falling within 10% of the GSD in both Easting and Northing and about 25% of the GSD in height. The orientation difference is well within 0.001 deg.

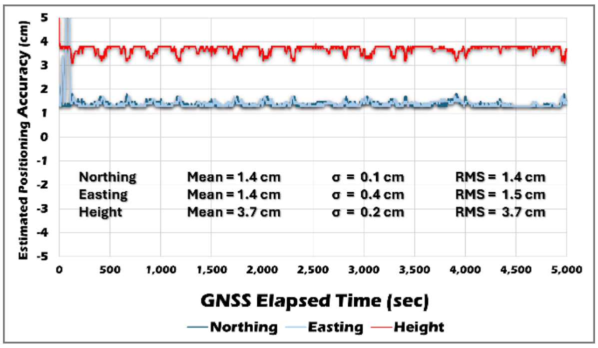

Figure 11: Estimated Positioning Accuracy Using Post Processed RTX - Greeley, CO, USA Dataset

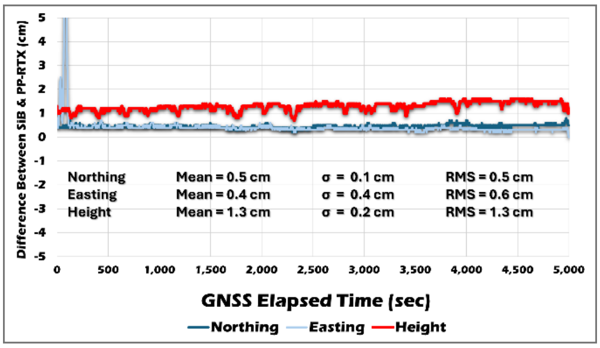

Figure 12: Difference between Single Base Processing and PP-RTX Processing - Greeley, CO, USA Dataset

3.1.2 Photogrammetric Workflow

Once the Smoothed Best Estimate of Trajectory (SBET) is established, image development and radiometric color balancing are executed within UltraMap, with the final color quality being highly dependent on SBET accuracy. Boresight calibration for the UltraCam Dragon's nadir and oblique cameras is subsequently performed using the tool Camera QC. Operating independently of ground control, Camera QC leverages the SBET data, the factory camera calibration parameters, and an automated, multi-camera tie point generation process (shown in Figure 12). To maintain geometric integrity while reducing computational overhead, a data thinning algorithm is applied. This restricts the dataset to robust tie points observed simultaneously (Figure 13) across all cameras and within the highest number of overlapping images, facilitating a unified relative adjustment.

Finally, POSPac applies the calibrated boresight angles to derive the final Exterior Orientation (EO) parameters. These refined EO parameters and images form the basis for subsequent mapping workflows, utilizing either Direct Georeferencing or light aerial triangulation prior to final map compilation. The adjusted EO parameters and corresponding imagery are subsequently imported into Trimble Photogrammetry to execute a light aerial triangulation, operating entirely without ground control. Following this adjustment, the geometric fidelity of the project is evaluated through a two-tiered accuracy assessment, comprising both orthophoto and stereoscopic evaluations.

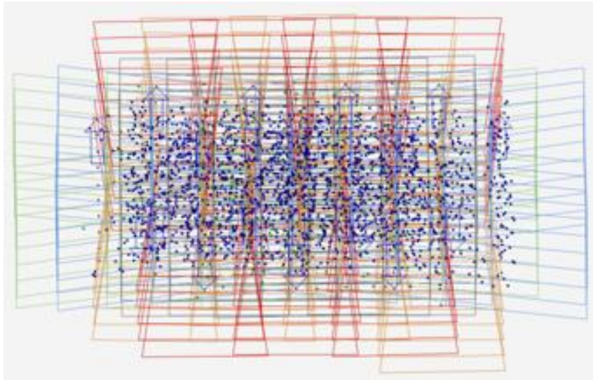

Figure 13: Tie Points Observed Simultaneously across all Cameras using Camera QC

To assess the accuracy of the orthoimagery, a total of 19 independent check points were utilized. Figure 14 illustrates the photogrammetric check point residuals for the Greeley, CO, USA dataset when employing the post-processed single base trajectory.

Similarly, the check point residuals derived from the PP-RTX trajectory are presented in Figure 15.

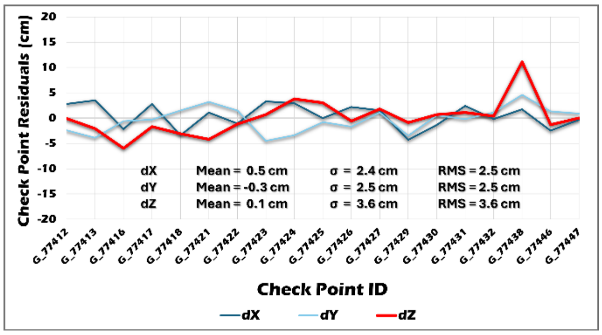

Figure 14: Photogrammetric Check Point Residuals Using Post-Processed Single Base Trajectory - Greeley, CO, USA Dataset

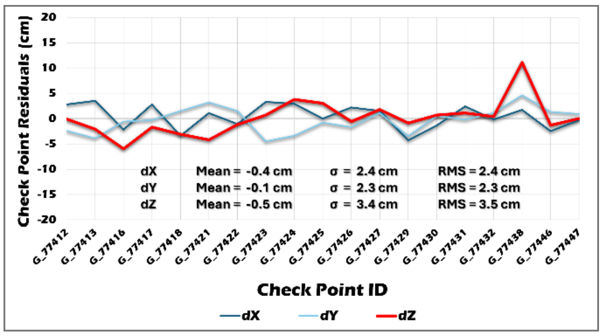

Figure 15: Photogrammetric Check Point Residuals Using Post-Processed RTX Trajectory - Greeley, CO, USA Dataset

For the stereoscopic accuracy assessment, the same 19 independent check points were evaluated across 289 distinct stereopairs.

Figure 16 illustrates the photogrammetric check point residuals for the Greeley, CO, USA dataset when employing the post-processed single base trajectory using direct georeferencing without AT or Datum Calibration. The corresponding residuals derived from the PP-RTX trajectory across these same 289 stereopairs are presented in Figure 17.

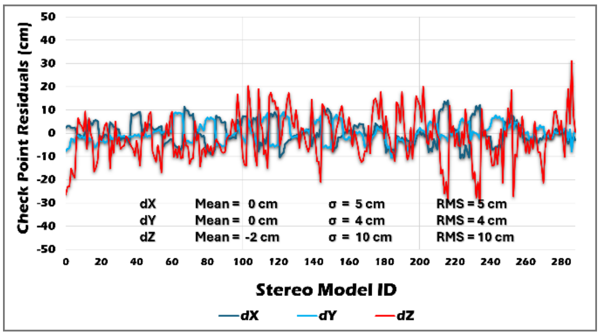

Figure 16: Check Point Residuals for 289 Stereopairs Using Single Base - Greeley, CO, USA Dataset

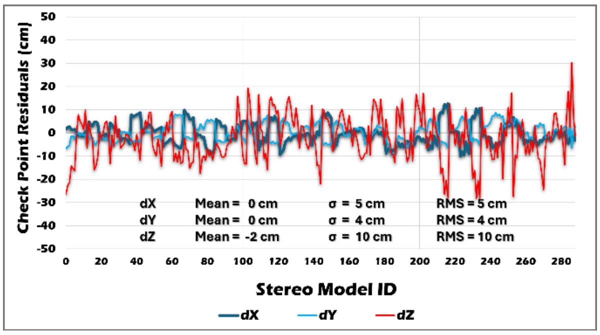

Figure 17: Check Point Residuals for 289 Stereopairs Using PP-RTX - Greeley, CO, USA Dataset

3.1.3 LiDAR Data Processing Workflow

The initial boresight calibration was executed within the RIEGL RiProcess environment. Following this step, LiDAR QC was employed to conduct a comprehensive optimization of the boresight and lever arm parameters, as well as the SBET itself. This refinement was achieved by processing the existing trajectory and the LiDAR point cloud data simultaneously.

For the final accuracy assessment of the LiDAR point cloud, the identical set of check points employed in the photogrammetric evaluation was retained.

Each point was measured within the generated point cloud and compared to its known reference coordinates to compute spatial discrepancies.

The resulting coordinate residuals are presented in Figure 18. The associated statistical measures of the check point residuals are listed in Table 3.

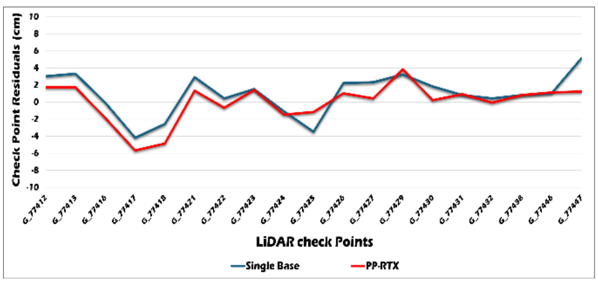

Figure 18: LiDAR Point Cloud Accuracy Assessment using Check Points for both Single Base and PP-RTX Greeley, Co Dataset

Table 3: LiDAR Check Point Statistics – Greeley, Co Dataset

Statistics (cm)	Single Base	PP-RTX
Minimum	-4	-6
Maximum	5	4
Mean	1	1
σ	2	2
RMS	**3**	**2**

3.2 Test Flight #2 (Gleisdorf, Austria)

To establish the repeatability and consistency of the UltraCam Dragon system, a second flight test was conducted in Gleisdorf, Austria. The flight trajectory, illustrated in Figure 19, was executed at a speed of 65 m/s and an approximate altitude of 1,000 m above ground level (AGL).

These flight parameters were specifically selected to yield a ground sample distance (GSD) of 5 cm and a LiDAR point density of 30 points per square meter. The resulting LiDAR point cloud, along with the spatial distribution of the 13 independent check points within the study area, is illustrated in Figure 20.

The resulting photogrammetric check point residuals for the Gleisdorf dataset are summarized in Table 4. Furthermore, the spatial discrepancies associated with the LiDAR data are visualized in Figure 21, while their comprehensive statistical metrics are tabulated in Table 5.

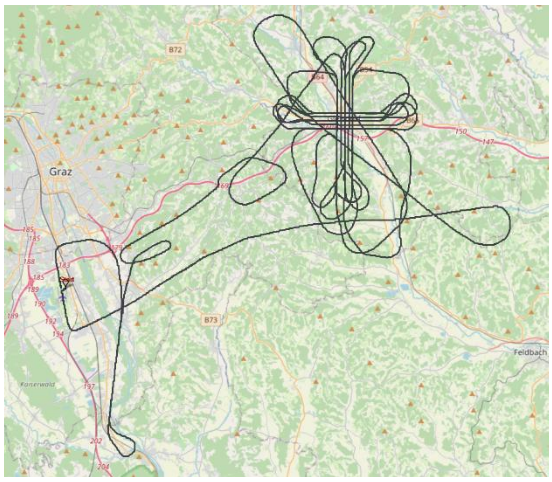

Figure 19: Test Flight Trajectory in Gleisdorf, Austria

Table 4: Photogrammetric Check Point Statistics (cm)

Check Point ID	dN (cm)	dE (cm)	dH (cm)
AH	0	0	2
BB	1	1	-2
BC	2	0	-3
BD	1	0	3
C_0121	1	-2	-1
GD003	1	3	-1
GD006	-3	1	-3
GD007	-2	-1	2
J_0177	0	-2	2
O_0217	-1	-1	-3
P_0085	3	4	6
Q_NEU	0	-1	-1
R_0209	-2	-1	1
σ	**1.7**	**1.8**	**2.7**
RMS	**1.7**	**1.8**	**2.8**

https://doi.org/10.5194/isprs-archives-XLIX-B1-2026-323-2026

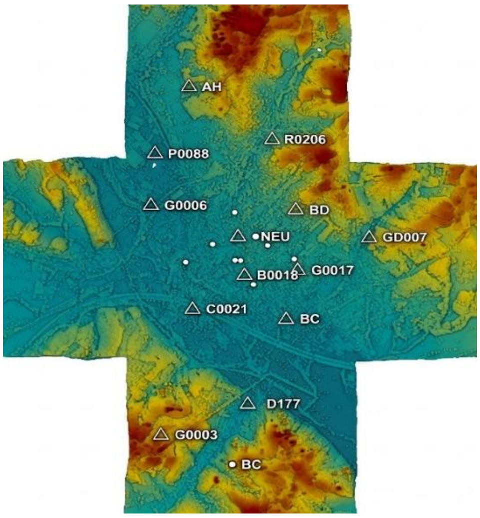

Figure 20: LiDAR Point Cloud – Gleisdorf, Austria Test Flight

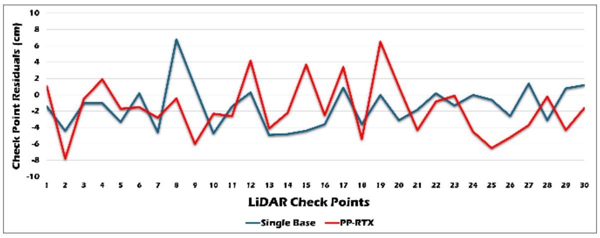

Figure 21: LiDAR Point Cloud Accuracy Assessment using Check Points for both Single Base and PP-RTX Gleisdorf, Austria Dataset

Table 5: LiDAR Check Point Statistics – Gleisdorf Dataset

Statistics (cm)	Single Base	PP-RTX
Minimum	-5	-8
Maximum	7	7
Mean	-1	-2
σ	3	3
RMS	**3**	**3**

4. SUMMARY AND CONCLUSIONS

This paper has introduced the UltraCam Dragon system, detailing its core components and outlining the associated data processing workflow.

To evaluate the system's performance, a thorough accuracy assessment was conducted using data from two independent test flights over Greeley, Colorado, USA, and Gleisdorf, Austria. The following points summarize the key observations derived from these missions:

- **Single Base Station Performance:** The estimated RMS positioning accuracy utilizing a single base station is approximately 20% of the GSD in both Northing and Easting, and approximately 50% of the GSD in height. Additionally, the forward-reverse separation RMS is well within 10% of the GSD.

- **PP-RTX Performance:** The estimated RMS positioning accuracy utilizing PP-RTX is approximately 30% of the GSD in both Northing and Easting, and roughly 75% of the GSD in height. PP-RTX not only provided sub-pixel accuracy but also eliminated the traditional logistical constraints associated with operating a single dedicated base station during airborne flights.

- **Hardware Compliance:** The estimated positioning accuracies for both the Single Base Station and PP-RTX methodologies fall well within the stringent accuracy specifications of the Trimble AP+ 60. This was repeatedly observed across both the Greeley and Gleisdorf test flights.

- **Trajectory Variance:** The absolute coordinate difference between the two computed trajectories is exceptionally minimal, falling within 10% of the GSD in both Easting and Northing, and about 25% of the GSD in height. The orientation difference is well within 0.001 degrees.

- **Photogrammetric Accuracy Assessment:** Independent check points were utilized to assess the spatial accuracy of the imagery for both test flights. The photogrammetric check point statistics proved consistent across both datasets, yielding an RMS within 0.5 GSD horizontally and 0.7 GSD vertically. These results were repeatable regardless of whether the Single Base Station or PP-RTX method was used for trajectory calculations.

- **Stereo Model Accuracy Assessment:** A total of 289 stereo models were evaluated in the Greeley dataset, while 208 stereo models were assessed in the Gleisdorf dataset. Both test flights demonstrated consistent stereoscopic accuracy, with the RMS ranging from 2 cm horizontally to 4 cm in height for both the Single Base and PP-RTX solutions.

- **LiDAR Accuracy:** The final LiDAR point cloud assessment, validated via check points, proved highly consistent between the two test flights, achieving an absolute accuracy of approximately 3 cm (roughly 0.6 GSD of the camera system) This level of precision reflects the overall accuracy of the LiDAR system and its rigorous sensor calibration, aligning perfectly with the absolute accuracy of the camera system.

- **USGS Quality Level:** Both datasets (Greely and Gleisdorf) meet USGS (U.S. Geological Survey, n.d.) 3DEP Quality Level 0 (QL0) as their aggregate nominal pulse spacing is ≤ 0.35 m (≥ 8 pulses/m²) and their swath relative vertical precision is ≤ 0.03 m, with ≤ 0.04 m inter-swath differences in overlap. They also satisfy QL0 absolute vertical accuracy by achieving non-vegetated RMSEz ≤ 0.050 m.

ACKNOWLEDGEMENT

Jason Woolard and Jon Sellars of the U.S. National Oceanic and Atmospheric Administration (NOAA) are gratefully acknowledged for their thorough testing of the latest Camera QC software, and for providing valuable feedback based on its use in their Rapid Response Operations. Vi Huynh is gratefully acknowledged for her thorough data processing and analysis of different Vexcel datasets using POSPac and Camera QC softwares.

REFERENCES

Casella, V., Jacobsen, K., Mostafa, M.M.R., and Franzini, M., 2006: A European project on direct georeferencing. Proceedings of the ASPRS Annual Conference, Reno, Nevada, USA, 1–5 May 2006.

Colomina, I., and Blazquez, M., 2014: Pose versus state: are sensor position and attitude sufficient for modern photogrammetry and remote sensing. The International Archives of the Photogrammetry, Remote Sensing and Spatial Information Sciences, XL-3/W1.

Dohr, S., Muick, M., Schachinger, B., and Gruber, M., 2022: Image motion compensation – The Vexcel approach. The International Archives of the Photogrammetry, Remote Sensing and Spatial Information Sciences, XLIII-B1-2022, 333–338.

Gruber, M., Schachinger, B., and Mostafa, M.M.R., 2022: The next generation Vexcel Imaging 3D city modelling using directly georeferencing data. The International Archives of the Photogrammetry, Remote Sensing and Spatial Information Sciences, XLIII-B1-2022, XXIV ISPRS Congress, 6–11 June 2022, Nice, France.

Gruber, M., and Wiechert, A., 2017: News from UltraCam sensors – an update. Proceedings of the ASPRS Annual Meeting (IGTF 2017), Baltimore, Maryland, USA, 12–16 March 2017.

Hutton, J., Mostafa, M.M.R., and Scherzinger, B., 2004: Inertial navigation systems. In: Manual of Photogrammetry, 5th edn., ASPRS, Bethesda, MD, USA, ISBN 1-57083-071-1.

Ip, A.W.L., Dillane, W., Giannelia, A., and Mostafa, M.M.R., 2006: Georeferencing of the UltraCam D images – boresight calibration results. Photogrammetric Engineering & Remote Sensing (PE&RS), 72(1): 9.

Ip, A.W.L., El-Sheimy, N., and Mostafa, M.M.R., 2007: Performance analysis of integrated sensor orientation. Photogrammetric Engineering & Remote Sensing (PE&RS), 73(1): 89–97.

Mostafa, M.M.R., and Hutton, J., 2004: A fully integrated solution for aerial surveys: design, development, and performance analysis. Photogrammetric Engineering & Remote Sensing (PE&RS), 71(4): 391–399.

Mostafa, M.M.R., and Schwarz, K.P., 2001: Digital image georeferencing from a multiple camera system by GPS/INS. ISPRS Journal of Photogrammetry and Remote Sensing, 56(1): 1–12.

Mostafa, M.M.R., 2001: Boresight calibration without ground control. Proceedings of the OEEPE Workshop on Integrated Sensor Orientation, Hanover, Germany, 17–18 September 2001.

Mostafa, M.M.R., and Schwarz, K.P., 1997: A fully digital system for airborne mapping. Proceedings of KIS97, Banff, Canada, 3–6 June 1997, pp. 463–471.

Scherzinger, B., Hutton, J., and Mostafa, M.M.R., 2018: Enabling technologies. In: Digital Elevation Model Technologies and Applications, 2nd edn., ASPRS, Bethesda, MD, USA, ISBN 1-57083-082-7.

Schwarz, K.P., Chapman, M.A., Cannon, M.E., and Gong, P., 1993: An integrated INS/GPS approach to the georeferencing of remotely sensed data. Photogrammetric Engineering & Remote Sensing (PE&RS), 59(11): 1167–1174.

U.S. Geological Survey (USGS), n.d.: Topographic Data Quality Levels (QLs). Available online: https://www.usgs.gov/3d-elevation-program/topographic-data-quality-levels-qls (accessed 28 March 2026).